Endothelial plasticity in fibrosis and epigenetics as a therapeutic target

Hulshoff, Melanie

DOI:
10.33612/diss.146265795

CHAPTER 3

HYPOXIA-INDUCED ENDOTHELIAL-MESENCHYMAL TRANSITION IS ASSOCIATED WITH RASAL1 PROMOTER HYPERMETHYLATION IN HUMAN CORONARY ENDOTHELIAL CELLS

Xingbo Xu[1,2], Xiaoying Tan[1,2], Melanie S. Hulshoff[1], Tim Wilhelmi[1], Michael Zeisberg[2,3] and Elisabeth M. Zeisberg[1,2]

[1]Department of Cardiology and Pneumology, University Medical Center of Göttingen, Georg-August University, Göttingen, Germany.
[2]German Centre for Cardiovascular Research (DZHK), Göttingen, Germany.
[3]Department of Nephrology and Rheumatology, University Medical Center of Göttingen, Georg-August University, Göttingen, Germany.

FEBS Lett 2016; 590(8): 1222-33.

ABSTRACT

Cardiac fibrosis is integral in chronic heart disease, and one of the cellular processes contributing to cardiac fibrosis is endothelial-to-mesenchymal transition (EndMT). We recently found that hypoxia efficiently induces human coronary artery endothelial cells (HCAEC) to undergo EndMT through a hypoxia inducible factor-1α (HIF1α)-dependent pathway. Promoter hypermethylation of Ras-Gap-like protein 1 (RASAL1) has also been recently associated with EndMT progression and cardiac fibrosis. Our findings suggest that HIF1α and transforming growth factor (TGF)/SMAD signalling pathways synergistically regulate hypoxia-induced EndMT through both DNMT3a-mediated hypermethylation of RASAL1 promoter and direct SNAIL induction. The findings indicate that multiple cascades may be activated simultaneously to mediate hypoxia-induced EndMT.

INTRODUCTION

Endothelial-to-mesenchymal transition (EndMT), which was originally described as cellular mechanism leading to formation of the mesenchymal cushion from AV-canal endothelial cells during cardiac development [1], has emerged as causal contributor in various pathologies, including in organ fibrosis involving heart or kidney, in brain vascular malformations or as source of fibroblasts in tumour stroma [2–10]. As the contribution of EndMT to these pathologies is increasingly being recognised, there is a growing number of identified EndMT-inducing stimuli, including various growth factors, environmental factors, such as hypoxia or high glucose, inflammation, direct cell–cell interactions or shear stress [11–17]. In context of fibrosis transforming growth factor β (TGFβ), hypoxia and Ras-GTP signalling have consistently emerged as inducers of EndMT; all of which are hallmarks of the fibrotic microenvironment.

Transforming growth factor β is the prototypical profibrotic growth factor, and inhibition of TGFβ signaling is one of the leading targets for antifibrotic drug development. Of the three known TGFβ isoforms, TGFβ1 and TGFβ2 can induce EndMT. TGFβ elicits signalling responses by binding to a type II receptor (TGFβR-II) which recruits and phosphorylates a type I receptor (activin-like kinase 5, ALK5) [18,19]. In addition to ALK5, ALK4 and ALK7 have also been found to activate the SMAD 2/3 signalling pathway [20]. The activated receptors then recruit and phosphorylate SMAD 2 and SMAD 3, which then bind to the common SMAD 4. Several studies have shown that activation of these TGFβ receptors type I is required for phosphorylation and consecutive action of Smad 2/3 and that Smad 2/3 alone without activation of the TGFβ receptor type I does not lead to Smad 2/3-induced gene regulation [21,22]. This heterodimeric Smad-complex then enters the nucleus, where it acts as a transcription factor. Among Smad-target genes are the transcription factors TWIST, SNAIL and SLUG, which all have been identified as inducers of EndMT.

Furthermore, long-term exposure to TGFβ1 induces aberrant CpG island promoter methylation of select genes, including RASAL1, encoding for the Ras-Gaplike protein 1 (RASAL1). RASAL1 converts (active) Ras-GTP to (inactive) Ras-GDP, and its transcriptional suppression through promoter methylation causes

increased intrinsic Ras-GTP activity, ultimately contributing to EndMT and fibrosis.

Hypoxia, the state of low oxygen concentration, is another hallmark of the fibrotic microenvironment, and several studies reported that hypoxia is a stimulus for endothelial cells to undergo EndMT [15,23–25]. Cellular responses to hypoxia are mediated by hypoxia inducible factors (HIFs), most prominently by HIF1, a highly conserved heterodimeric complex composed of an alpha (HIF1α) and a beta subunit (HIF1β, syn. aryl hydrocarbon receptor nuclear translocator ARNT). Under normoxic conditions, the alpha subunit of HIF is hydroxylated by HIF prolyl-hydroxylases, allowing their ubiquitination and rapid degradation. In hypoxic conditions, HIF accumulates because prolyl-hydroxylase is inhibited [26,27]. HIF-1 acts by binding to HIF-responsive elements (HREs) in promoters that contain the sequence NCGTG [28]. In this regard, we had previously established that hypoxia induces EndMT via direct induction of the transcription factor SNAIL [15].

While all three EndMT pathways were identified as single EndMT stimuli in cell culture experiments, cells are simultaneously exposed to all three of them within fibrotic tissue and crosstalk between the pathways is not yet understood. Here, we explore possible contribution of TGFβ-signalling and RASAL1 CpG island promoter methylation in hypoxia-induced EndMT in human coronary artery endothelial cells.

RESULTS

HYPOXIA INDUCES RASAL1 CPG ISLAND PROMOTER METHYLATION AND ENDMT

To explore possible involvement of RASAL1 CpG island promoter methylation in hypoxia-induced EndMT, we exposed human coronary artery endothelial cells (HCAEC), which have been extensively characterised as a population of homogeneous endothelial cells in previous studies [15], to hypoxia. After 3 days of hypoxia, HCAEC acquired a spindle-shaped morphology (Fig. 1A) associated with decrease in endothelial cell marker CD31 and increased expression of mesenchymal markers S100A4 and alpha-smooth muscle actin (*α*SMA) and accumulation of HIF1α (Fig. 1B–D), reminiscent of endothelial cells undergoing

an EndMT. Such EndMT was associated with increased expression of transcription factors SNAIL, SLUG and TWIST (Fig. 1E), in line with previous studies. Such hypoxia-induced EndMT was further associated with increased Ras-GTP activity (Fig. 1F), decreased RASAL1 expression (Fig. 1G) and increased degree of RASAL1 CpG island promoter methylation (Fig. 1H).

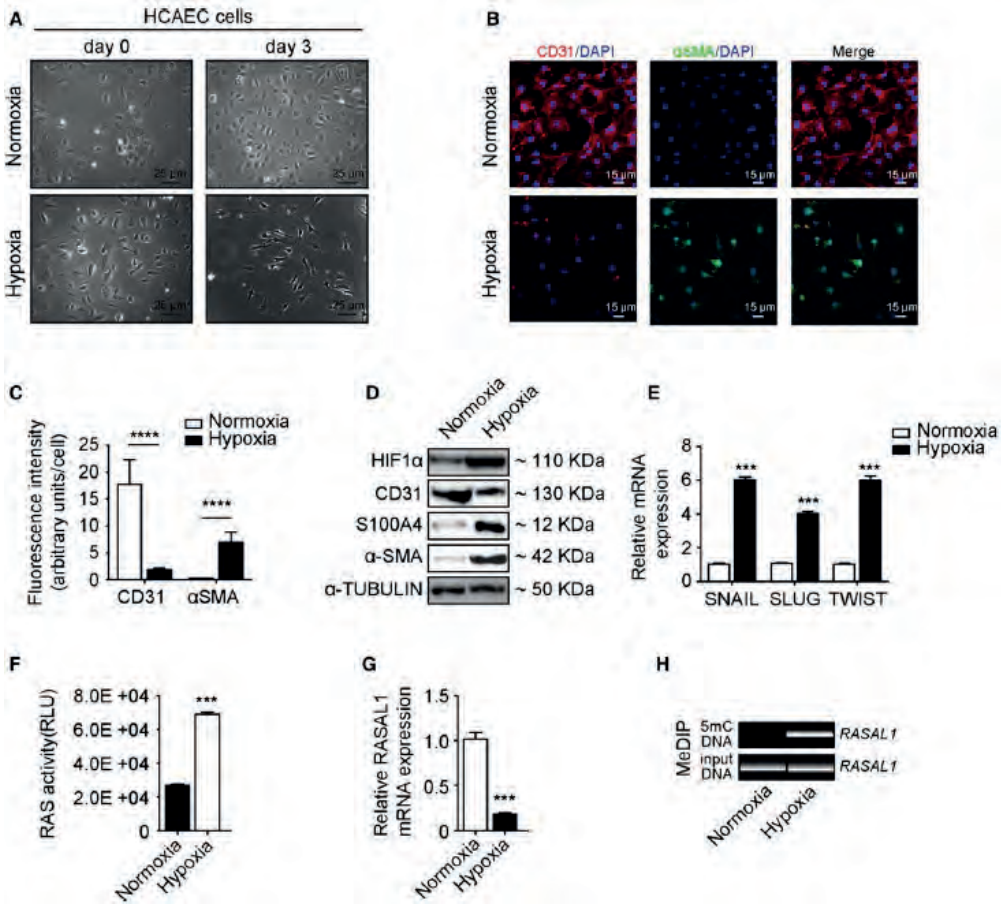

Figure 1. Hypoxia induces RASAL1 promoter hypermethylation in HCAEC.

*(A) Phase-contrast microscopy pictures showing that cell morphology of HCAEC cells which were incubated under normoxic (upper) and hypoxic condition (lower) for 3 days. Scale bar equals 25 µm. (B) Representative immunofluorescence images showing CD31 (red) and α-SMA (green) staining in cell exposure to normoxia (upper panel) and hypoxia (lower panel); nuclei were counterstained with DAPI (blue). Scale bars 15 µm. (C) Densitometric measurements of the fluorescence signal of CD31 and α-SMA from images B using the IMAGEJ software. The arbitrary units of fluorescence signal were measured from single cells and represented by mean value. Error bars represent standard deviation, ****P < 0.0001. (D) Western blot analysis showing protein expression of HIF1α, CD31,*

*S100A4 and α-SMA in HCAEC cells under normoxic and hypoxic conditions. All blots were reprobed with an anti-α-TUBULIN antibody as a control for equal loading. (E) qRT-PCR data showing the mRNA expression of key EndMT transcriptional factors (SNAIL, SLUG, and TWIST) in normoxic and hypoxic cells. All three genes were significantly increased upon hypoxic condition (gene expression and associated error bars, representing mean ± SEM, n = 3 independent experiments, ***P < 0.001). (F) RAS activity was measured by ELISA assay, cells cultured under normoxic condition served as controls. Hypoxia-treated cells showing RAS hyperactivity (data are presented as mean ± SEM, n = 6 independent experiments, ***P < 0.001). (G) qRT-PCR data showing the reduction in RASAL1 mRNA expression in hypoxia-treated cells (gene expression and associated error bars, representing mean ± SEM, n = 3 independent experiments, ***P < 0.001). (H) DNA virtual gel pictures showing the MeDIP results of enriched methylated DNA in RASAL1 promoter region in HCAEC cells exposed to hypoxic condition.*

Under pathological conditions, microvascular endothelial cells are a major cellular population contributing to EndMT. Therefore, in order to rule out the possibility that microvascular endothelial cells differ from macrovascular endothelial cells in response to hypoxia, we have repeated the experiments with human coronary microvascular endothelial cells (HCMEC) and obtained similar results (Fig. 2). In summary, we observed that hypoxia-induced EndMT is associated with increased RASAL1 promoter methylation and subsequent Ras-GTP activity. While this observation was in line with previous studies, which had established that RASAL1 CpG island promoter methylation is causally involved in TGFβ-induced EndMT, we next aimed to gain insights into the mechanism which mediates aberrant promoter methylation in response to hypoxia.

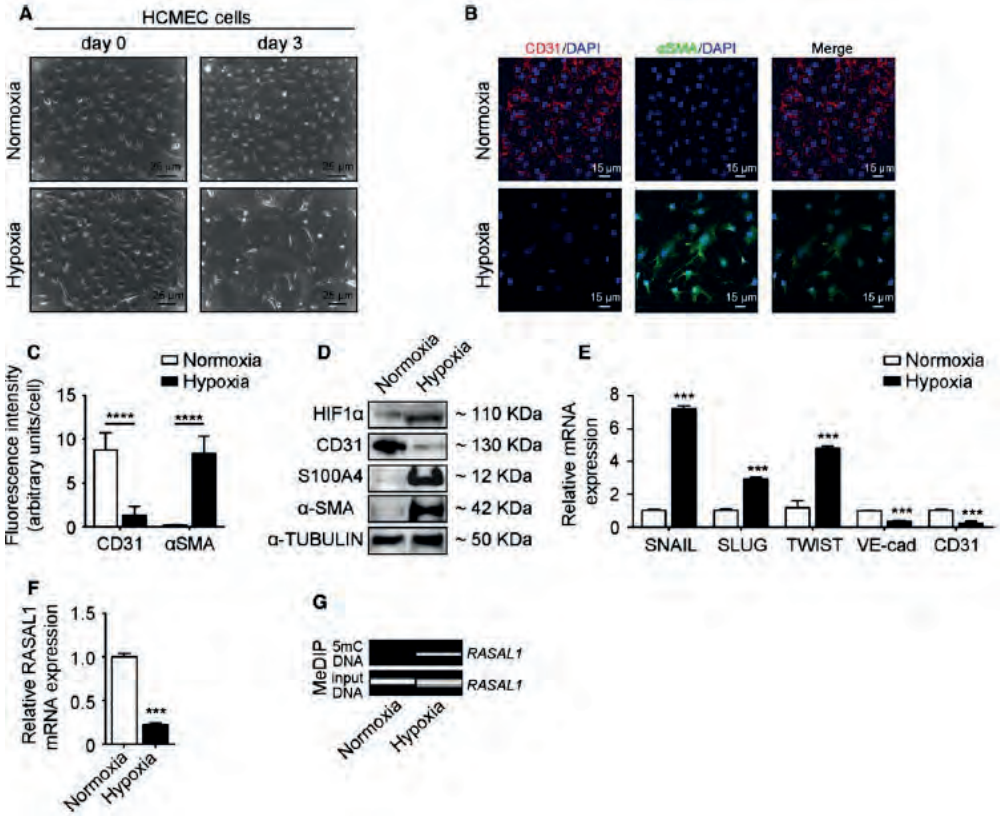

Figure 2. Hypoxia induces RASAL1 promoter hypermethylation in HCMEC.

*(A) Phase-contrast microscopy pictures showing cell morphology of HCMEC cells which were incubated under normoxic (upper) and hypoxic condition (lower) for 3 days. Scale bar equals 25 µm. (B) Representative immunofluorescence images showing CD31 (red) and α-SMA (green) staining in cells exposed to normoxia (upper panel) or hypoxia (lower panel); nuclei were counterstained with DAPI (blue). Scale bars 15 µm. (C) Densitometric measurements of the fluorescence signal of CD31 and α-SMA from images B using IMAGEJ software. Arbitrary units of fluorescence signal were measured from single cells and represented by mean value. Error bars represent standard deviation, ****P < 0.0001. (D) Western blot analysis showing protein expression of HIF1α, CD31, S100A4, α-SMA in HCAEC cells under normoxic or hypoxic conditions. All blots were reprobed with an anti-α-TUBULIN antibody as a control for equal loading. (E) qRT-PCR data showing the mRNA expression of key EndMT transcriptional factors (SNAIL, SLUG and TWIST) and endothelial cell markers (VE-cadherin and CD31) in normoxic and hypoxic cells. (gene expression and associated error bars, representing mean ± SEM, n = 3 independent experiments, ***P < 0.001). (F) qRT-PCR data showing the reduction in RASAL1 mRNA expression in hypoxia-treated cells (gene expression and associated error bars, representing mean ± SEM, n = 3 independent experiments, ***P < 0.001). (G) DNA virtual gel pictures showing the MeDIP results of enriched methylated DNA in RASAL1 promoter region in HCMEC cells exposed to hypoxic condition.*

HYPOXIA-INDUCED RASAL1 CPG ISLAND PROMOTER METHYLATION IS FACILITATED BY DNMT3A

In principle, four enzymes (Dnmt1, Dnmt3a, Dnmt3b and Dnmt3l) with DNA-methylating activity are known in humans. As previous studies established that DNA methylation through either of these enzymes is dependent on their transcriptional activities, we next analysed expression of DNMTs in HCAEC upon exposure to hypoxia by quantitative real-time PCR. Among the four DNMTS members, only expression of DNMT3a was substantially increased (Fig. 3A–D). To explore causal involvement of DNMT3a in hypoxia-induced RASAL1 methylation, we performed siRNA-mediated DNMT3a knockdown, sufficiently depleting intracellular DNMT3a (Fig. 3E,F) without influencing the expression of other DNMT family members (Fig. 3G). Silenced DNMT3a expression did not affect the expression of endothelial cell marker gene CD31 nor fibroblast specific genes S100A4 and αSMA (Fig. 3H) under normoxic condition. DNMT3a-depletion blunted suppression of RASAL1 expression in response to hypoxia (Fig. 3I) and RASAL1 CpG island promoter methylation (Fig. 3J), but did not completely abolish the effect of hypoxia on RASAL1 expression and promoter methylation. DNMT3a depletion also blunted induction of SNAIL, SLUG and TWIST in response to hypoxia (Fig. 3K).

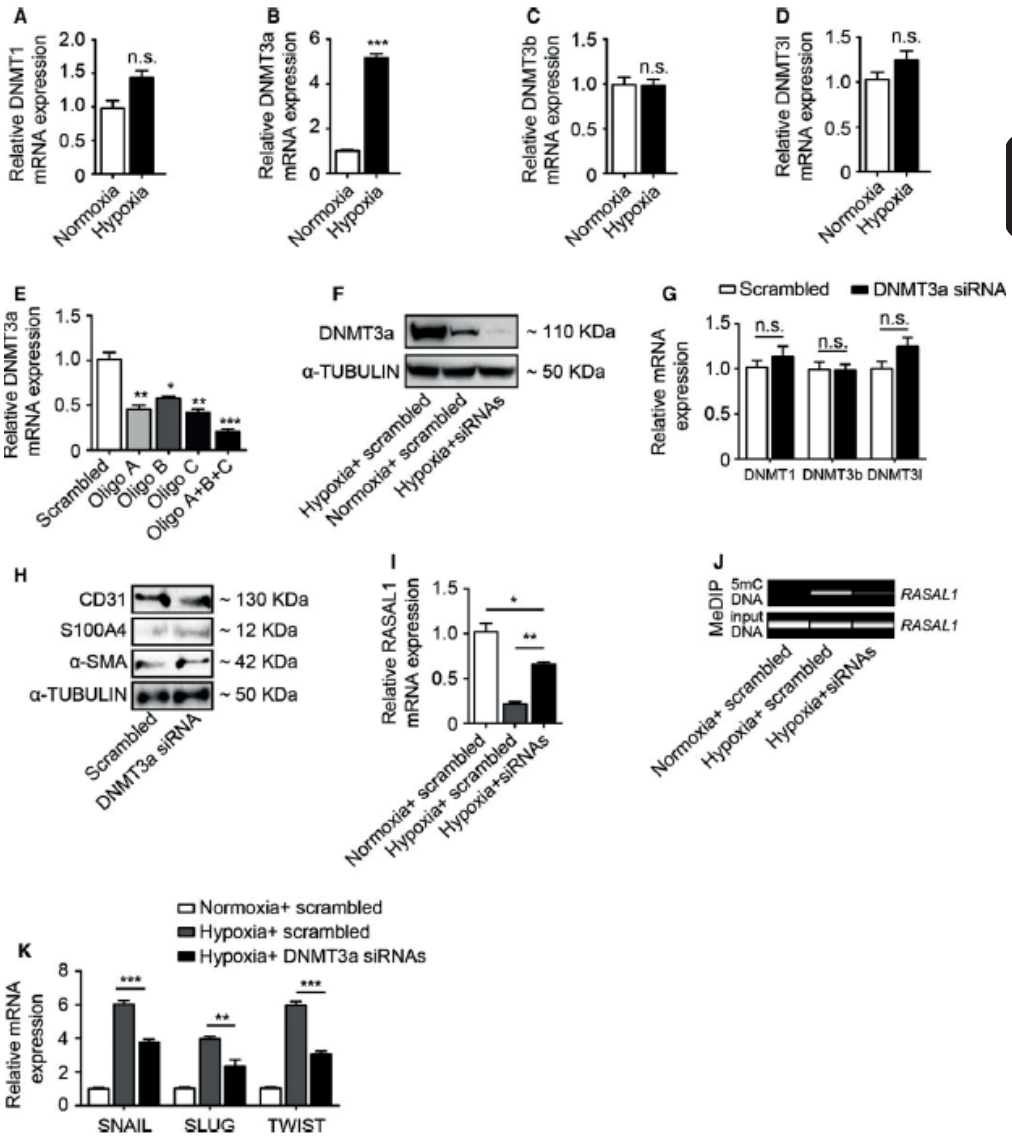

Figure 3. Silencing of DNMT3a expression alleviates hypoxia-induced EndMT.

(A–D) qRT-PCR results showing the mRNA expression of DNA methyltransferases (DNMT1, DNMT3a, DNMT3b and DNMT3l) in normoxic and hypoxic cells. DNMT3a is significantly upregulated upon hypoxia treatment. (E) qRT-PCR results showing DNMT3a mRNA expression in the cells which were transfected with different DNMT3a siRNA oligos. The combination of all three oligos contributed to over 70% reduction in DNMT3a. (F) Western blot results showing increased DNMT3a protein expression under hypoxic condition but not under normoxic condition, both transfected with combined DNMT3a. DNMT3a siRNAs treatment under hypoxic condition abolished expression of DNMT3a. (G) qRT-PCR results showing DNMT1, DNMT3b, and DNMT3l mRNA expression in HCAEC

*cells transfected with DNMT3a siRNA compared to cells transfected with scrambled control. (H) Western blot analysis showing protein expression of CD31, S100A4, α-SMA in DNMT3a siRNA transfected cells compared to scrambled control transfected cells. All blots were reprobed with an anti-α-TUBULIN antibody as a control for equal loading. (I) qRT-PCR results showing DNMT3a mRNA expression in cells transfected with scrambled controls siRNA treated with normoxia and hypoxia and cells transfected with combined DNMT3a siRNAs treated with hypoxia. (J) DNA virtual gel pictures showing the MeDIP results of decreased methylation level of immunoprecipitated RASAL1 promoter in DNMT3a siRNA transfected cells compared to scrambled control transfected cells under hypoxic condition. (K) qRT-PCR data showing mRNA expression of the key EndMT transcription factors (SNAIL, SLUG, and TWIST) in DNMT3a siRNA transfected cells as compared to scrambled control transfected cells exposed to hypoxic condition (gene expression and associated error bars, representing mean ± SEM, n = 3 independent experiments, n.s., no significance, *P < 0.05, **P < 0.01, ***P < 0.001).*

HYPOXIA INDUCES AUTORCRINE TGFβ SIGNALLING IN HCAEC

Because several previous studies had established TGFβ signalling as prototypical stimulus for EndMT and also as inducer of RASAL1 CpG island promoter methylation, we next aimed to explore possible involvement of TGFβ signalling in hypoxia-induced EndMT. For this reason, we first analysed expression of TGFβ1 (Fig. 4A), TGFβ2 (Fig. 4B) and TGFβ3 (Fig. 4C) by quantitative real-time PCR. Among the TGFβ isoforms, expression of TGFβ2 was significantly increased upon exposure to hypoxic conditions. Furthermore, we also detected a significant increase in secreted TGFβ2 by ELISA assay in the supernatant of cells collected 3 days after hypoxia treatment (Fig. 4D). Corresponding with increased TGFβ2 expression, intracellular levels of phosphorylated SMAD2 (Fig. 4E) and of phosphorylated SMAD3 (Fig. 4F), both indicative of active TGFβ signalling, were increased. Activated SMAD signalling was also shown by an increased expression of the SMAD-target gene PAI-I (Fig. 4G).

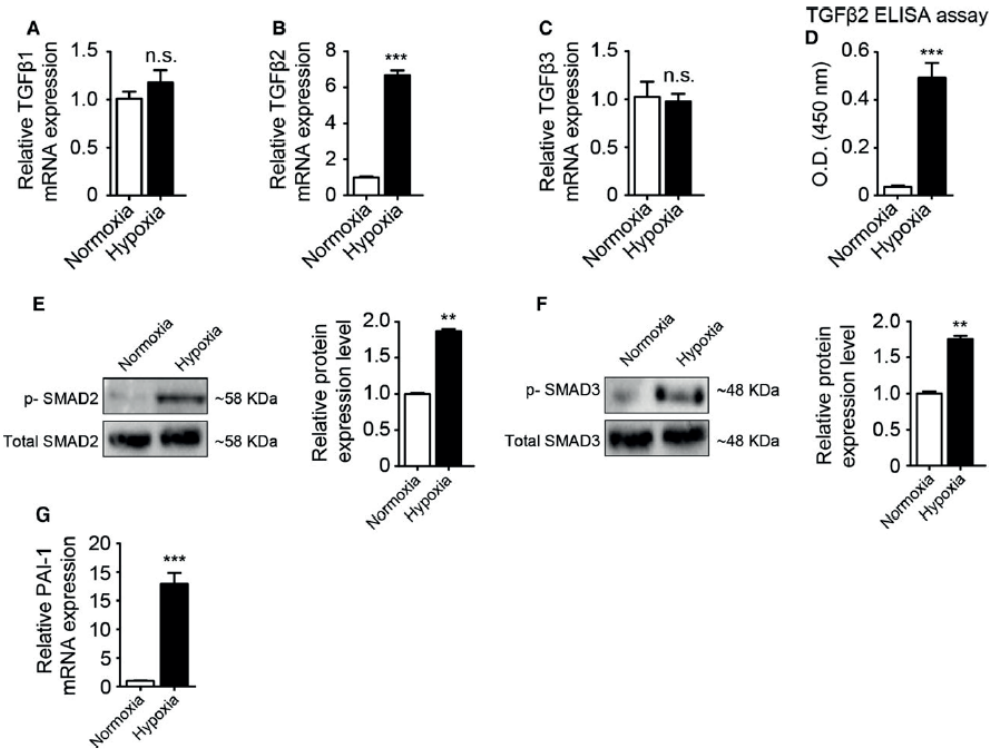

Figure 4. Hypoxia activates SMAD signaling pathway through inducing TGFb2 expression.

*(A–C) qRT-PCR results showing mRNA expression of all three TGFβ isoforms (TGFβ1, TGFβ2, and TGFβ3) in normoxic and hypoxic cells. TGFβ2 mRNA expression was significantly increased upon hypoxia treatment (gene expression and associated error bars, representing mean ± SEM, n = 3, n.s., no significance, ***P < 0.001). (D) ELISA assay measured the TGFb2 in the cell medium secreted form cells exposed to hypoxia for 3 days. (E–F) Western blot analysis showing activated SMAD2 (E) and activated SMAD3 (F) proteins in hypoxic cells detected by specific antibodies against for phosphorylated SMADs. The membranes were reprobed by total SMAD2 or total SMAD3 antibodies for equal-loading control. The expression levels were quantified by densitometry analysis (protein expression and associated error bars, representing mean ± SD, n = 3, **P < 0.01). (G) qRTPCR results showing mRNA expression of a SMAD target gene, PAI-1 in normoxic and hypoxic cells. (gene expression and associated error bars, representing mean ± SEM, n = 3, ***P < 0.001).*

AUTOCRINE TGFβ SIGNALLING IS CAUSALLY INVOLVED IN HYPOXIA-INDUCED RASAL1 CPG ISLAND PROMOTER METHYLATION

To explore causal involvement of TGFβ signalling in RASAL1 CpG island promoter methylation, we next established a system enabling us to either overexpress FLAG-tagged SMADs-2, -3 and -4 (Fig. 5A-C), and to effectively deplete SMADS by siRNA-mediated knockdown (Fig. 5D,E). Combined SMAD overexpression to enhance TGFβ signalling responses further enhanced transcriptional suppression of RASAL1 (Fig. 5F) and RASAL1 CpG island promoter methylation (Fig. 5G) in response to hypoxia, whereas combined depletion of Smads-2 and -4 blunted the effect (but did not completely abolish it) on RASAL1 mRNA expression (Fig. 5H) and RASAL1 CpG island promoter methylation (Fig. 5I).

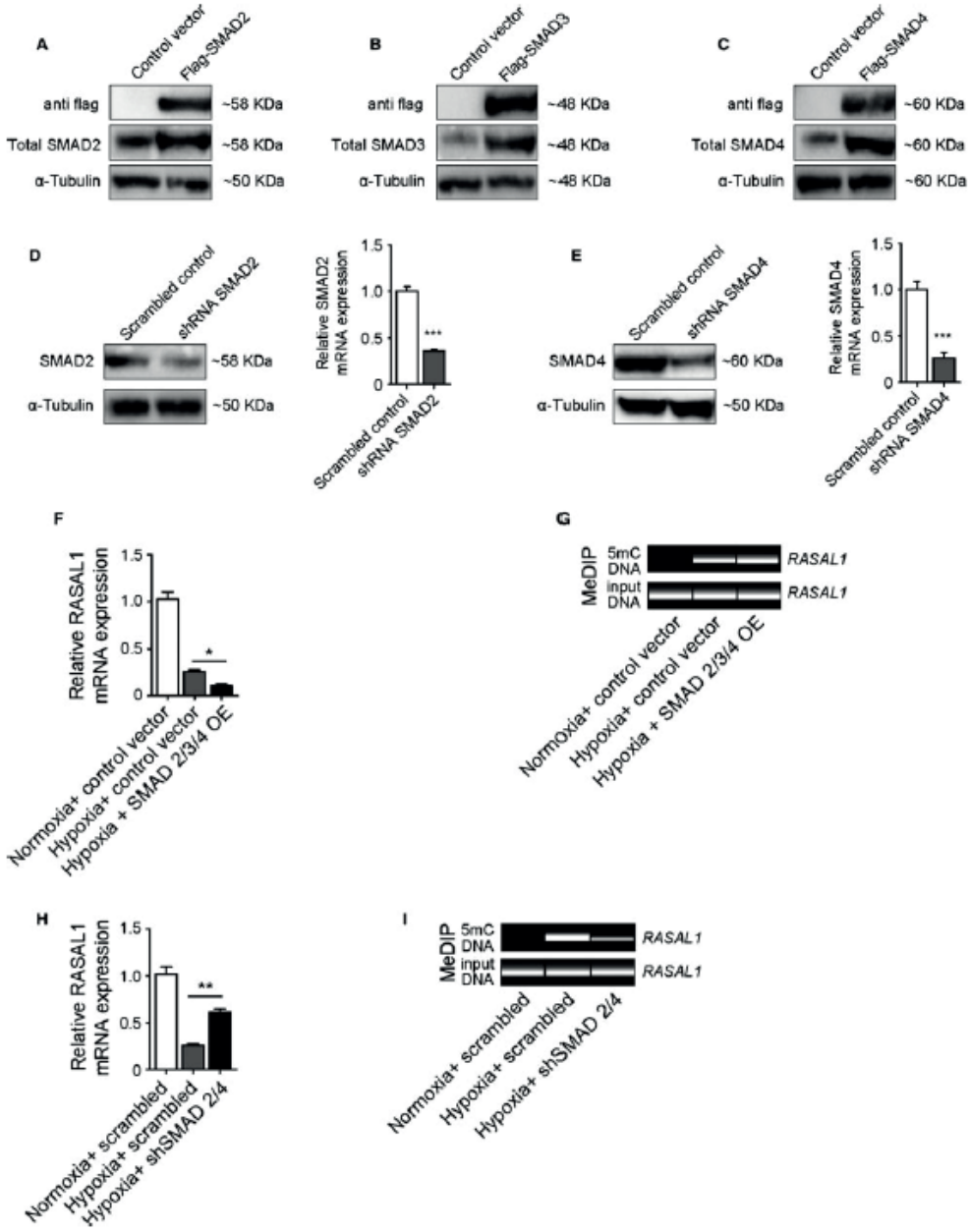

Figure 5. Silencing SMAD protein expression decreases hypoxia-induced RASAL1 promoter methylation.

(A–C) Western blot analysis showing SMAD2 (A), SMAD3 (B) and SMAD4 (C) expression in HCAEC cells which were transfected by overexpression constructs, pcDEF3-Flag(N)-hSmad2(C), pcDEF3-Flag(N)-hSmad3(D) and pcDEF3-Flag(N)-hSmad4(E). The expression levels of each protein were detected by flag antibody and corresponding antibodies. The membranes were reprobed with a-

*Tubulin antibody for equal-loading control. (D–E) SMAD2 (D) and SMAD4 (E) expression silencing using shRNA constructs. The expression levels were analysed by qRT-PCR and Western blots analysis. The total SMAD2 and SMAD4 protein were significantly reduced upon shRNA-transfected cells compared with scrambled control shRNA-transfected cells. The protein expression levels were quantified by densitometry analysis (protein expression and associated error bars, representing mean ± SD, n = 3, ***P < 0.001). (F) HCAEC cells were co-transfected with SMAD (SMAD2, SMAD3 and SMAD4) overexpression constructs, showing further decreased RASAL1 mRNA expression by qRT-PCR analysis (gene expression and associated error bars, representing mean ± SEM, n = 4, *P < 0.05). (G) DNA virtual gel pictures showing increased RASAL1 promoter methylation measured by MeDIP analysis. This correlates with the decrease in RASAL1 mRNA expression. (H) qRT-PCR results showing restored RASAL1 mRNA expression after silencing SMAD (SMAD2, SMAD4) proteins (gene expression and associated error bars, representing mean ± SEM, n = 4, **P < 0.01). (I) DNA virtual gel pictures showing reduced RASAL1 promoter methylation measured by MeDIP analysis. This correlates with the restored RASAL1 mRNA expression.*

DISCUSSION

Our study corroborates that hypoxia induces EndMT in HCAEC and provides evidence that such EndMT in response to hypoxia is mediated by at least two distinct signalling pathways, which cannot fully compensate for each other's absence (Fig. 6). Specifically, we here demonstrate that hypoxia induces autocrine TGFβ signalling, in addition to direct SNAIL activation by HIF1α. Notably, it is specifically TGFβ2 which is upregulated among the TGFβ-family members on mRNA level, and which is also detected as mature TGFβ2 in the secretome of endothelial cells upon hypoxia. While in context of fibrosis, the most abundant isoform within fibrotic tissue which had been identified as EndMT-inducing stimulus was TGFβ1 [29]. Our observation here is in line with several previous publications which identified TGFβ2 as most potent EndMT-inducing stimulus (without negating EndMT-inducing potential of TGFβ1) [30–32]. Our studies further demonstrate that hypoxia-induced autocrine TGFβ signalling leads to CpG island promoter methylation of RASAL1 and subsequently increased intrinsic RAS-GTP activity. While this observation is in line with our previous studies which demonstrated that TGFβ1-induced EndMT is causally mediated by RASAl1 methylation, it is notable that in this context of hypoxia such aberrant CpG island promoter methylation was specifically mediated by the methyltransferase Dnmt3a. Knockdown of DNMT3a via siRNA on the other hand

had no effect on EndMT, suggesting that DNMT3a plays no role with respect to EndMT under normoxic condition. While this confirms previous studies which identified specifically DNMT3a to be primarily responsible for de novo promoter methylation, this is in contrast to reports which had discovered Dnmt1 as the methyltransferase responsible for aberrant RASAL1 promoter methylation in context of fibrotic kidney fibroblast activation [33–36]. While these findings are not preclusive, it is attractive to speculate that DNMT1, which was originally identified to maintain methylation patterns by copying information onto the unmethylated strand in newly synthesized hemimethylated DNA, acts predominantly in actively proliferating fibroblasts, whereas Dnmt3a acts predominantly in context of nonproliferative EndMT. Importantly, depletion of Dnmt3a or of Smad-signalling only partially inhibited RASAL1 methylation, most likely due to incomplete knockdown, but also allowing for speculation that additional mechanisms are involved. Importantly, we are aware that other genes, in addition to RASAL1, are affected. We are further aware that EndMT likely occurs context-dependent, and that robust TGFβ and/or hypoxia stimulus is needed. In this context, a recent study has shown no contribution of EndMT in the model of transverse aortic constriction (TAC), 4 weeks after TAC (in this model robust hypertrophy occurred with modest fibrosis) [37], whereas in the more robust fibrosis model of ascending aortic constriction (AAC), about one-third of all fibroblasts were found to be of endothelial origin [6]. Therefore, further studies are needed to identify which stimuli induce EndMT under which circumstances.

ACKNOWLEDGEMENTS

This work was supported by DFG grants SFB1002/C01 (to EZ) and ZE523/4-1 (to MZ) and funds from the University of Göttingen Medical Center (UMG) to EZ and MZ. XX was supported by the ‘seed funding research program’ of the Faculty of Medicine, Georg-August University Göttingen and postdoc start-up grant, DZHK.

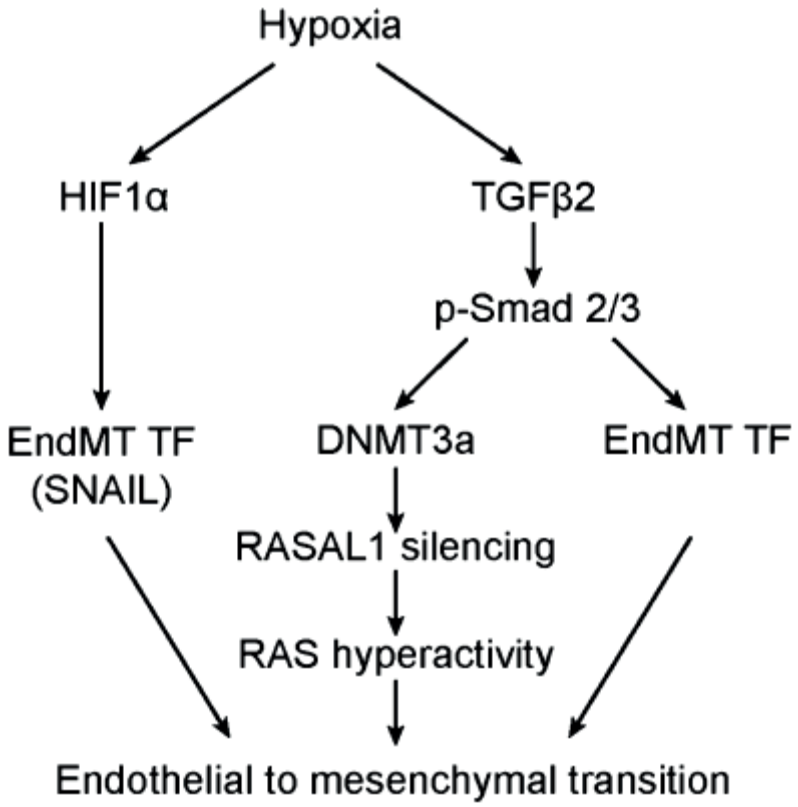

Figure 6. Hypoxia induces EndMT in HCAEC cells through different pathways. *Schematic representation of hypoxia-induced endothelial-to-mesenchymal transition through different cascades. Under hypoxic condition, transcription factor HIF1α protein is stabilised, which can directly activate EndMT transcriptional factor, Snail, to trigger the EndMT program. Besides, hypoxia can also activate TGFβ2 receptor regulated signalling pathway through SMAD2/3 proteins to induce EndMT transcription factor expression. In addition, we identified that hypoxia synergistically induces EndMT by DNMT3a-mediated hypermethylation of RASAL1 with consecutive Ras hyperactivity.*

MATERIALS AND METHODS

CELL CULTURE AND HYPOXIA INCUBATIONS

Human coronary artery endothelial cells (HCAEC) were obtained from Genlantis (San Diego, CA, USA) and maintained in HCAEC growth medium (Genlantis). Human microvascular endothelial cells (HCMEC) were purchased from Promocell (Heidelberg, Germany) and maintained in endothelial cell growth medium MV (Heidelberg, Germany). Both cell types were kept in an incubator at 37 °C with 5% CO_2 and medium was changed in every other day. A total of $1x10^6$ cells were preseeded onto 10 cm plates (Griner, Frickenhausen, Germany) and were incubated for 24 h before exposure to hypoxic incubation for 72 h. Hypoxic conditions were induced as previously described. Briefly, cell dishes were placed into a hypoxia chamber (STEMCELL Technologies, Kloen, Germany), and the inside air was purged by a gas mixture (containing 1% O2, 98% N2) for 5 min with 1 bar flow rate. The cell morphology was examined by phase-contrast microscopy (Zeiss Axiovert200 and AXIOVISION 3.0 software (Zeiss, Goettingen, Germany). The acquired imaged were processed using PHOTOSHOP CS3 software, Adobe, San Jose, CA, USA).

TRANSFECTION AND GENERATION OF PLASMID DNA CONSTRUCTS

For transfection, HCAEC cells were seeded at a confluence of 60–70% in a 10 cm dish and were cultured in growth medium overnight. Transfection was performed with Lipofectamine 2000 (Life Technologies, Paisley, UK) according to the manufacturer's instructions. Briefly, 5 µg of plasmid DNA from the respective constructs or 500 pmol of each siRNA oligo were incubated with Opti-MEM (Life Technologies) to a volume of 500 µL, and then mixed with 10 µL Lipofectamine plus Opti-MEM to a volume of 500 µL bringing the final volume to 1 mL. This mixture was incubated at room temperature for 20 min. Then the complex was added into the cell culture dish which contains 6 mL of endothelial basic medium (serum-free) for 4 h. Then, the transfection reagent-containing medium was removed and replaced by endothelial growth medium and the cells were exposed to hypoxic condition. For gene silencing experiment, DNMT3a siRNAs were purchased from OriGene (Rockville, MD, USA). pLKO.1 vector was used for

generating of pLKO.1-shSMAD2 (CCAGCAGGAATTGAGCCACAGAGTAATTA), pLKO.1-shSMAD4 (CCAACATTCCTGTGGCTTCCACAAGTCAG) constructs. For gene overexpression, the DNA plasmids, pcDEF3-Flag(N)-hSmad2, pcDEF3-Flag(N)-hSmad3 and pcDEF3-Flag(N)-hSmad4, were kindly provided by Prof. Miyazono as gifts [38].

RNA EXTRACTION AND QUANTITATIVE REAL-TIME PCR

Total RNA was extracted from cells using PureLink RNA kit (Life Technologies, Carlsbad, CA, USA) following the manufacturer's protocol. A quantity of 1 µg of total RNA was first digested with DNase I (Sigma-Aldrich, St. Louis, CA, USA) and the digested product was used for cDNA synthesis using the SuperScriptII system (Life Technologies). A qRT-PCR assay was performed as previously described [35]. Briefly, 2 µL of diluted cDNA (1/20) was used as a template in Fast SYBR Master Mix (Life Technologies) and run on a StepOne Plus realtime PCR system (Life Technologies) with the real-time PCR primers (sequence listed below). Measurements were standardized to the GAPDH reaction using delta delta Ct methods.

Gene	Sequence	Supplier
CD31	F: AAGGAACAGGAGGGAGAGTATTA R: GTATTTTGCTTCTGGGGACACT	Primer design Southampton, UK
DNMT1	F: TTCTGTTAAGCTGTCTCTTTCCA R: TGCTGAAGCCTCCGAGAT	Saha et al. [39]
DNMT3a	F: ATAGATCCCGGTGTTGAGCC R: ACCCAGCGCAGAAGCAG	Primer design Southampton, UK
DNMT3b	F: TCTCCATTGAGATGCCTGGT R: GAGATTCGCGAGCCCAG	Saha et al. [39]
DNMT3l	F: GCCGTACACAAGATCGAAGG R: GTTCTGACCCGGGACAACT	Minami et al. [40]
GAPDH	Undisclosed	Primer design Southampton, UK
PAI-1	F: GGCCATTACTACGACATCCTG R: GGTCATGTTGCCTTTCCAGT	Hao et al. [41]
RASAL1	F: CGTGCTGGATGAGGACACTG R: TCCCTGCTCAGCGAGATCTT	Primer design Southampton, UK
SLUG	F: ACTCCGAAGCCAAATGACAA R: CTCTCTCTGTGGGTGTGTGT	Primer design Southampton, UK
SMAD2	F: GGAGCAGAATACCGAAGGCA R: CTTGAGCAACGCACTGAAGG	Yu et al. [42]
SMAD4	F: TGGCCCAGGATCAGTAGGT R: CATCAACACCAATTCCAGCA	Wang et al. [43]
SNAIL	F: GGCAATTTAACAATGTCTGAAAAGG	Primer design Southampton, UK

	R: GAATAGTTCTGGGAGACACATCG	
TGFβ1	F: CACTCCCACTCCCTCTCTC R: GTCCCCTGTGCCTTGATG	Primer design Southampton, UK
TGFβ2	F: TACGCCAAGGAGGTTTACAAA R: TGAAGTAGGGTCTGTAGAAAGTG	Primer design Southampton, UK
TGFβ3	F: ACTATGCCAACTTCTGCTCAG R: CAGATGCTTCAGGGTTCAGA	Primer design Southampton, UK
TWIST	F: CTCAAGAGGTCGTGCCAATC R: CCCAGTATTTTTATTTCTAAAGGTGTT	Primer design Southampton, UK

PROTEIN EXTRACTION AND WESTERN BLOTTING

Proteins were extracted from cells and tissues using NP40 lysis buffer (Life Technologies), containing protease inhibitor cocktail (Roche, Mannheim, Germany). Western blotting assay was performed as previously described [44]. Protein samples were resolved on 4–12% SDS/PAGE and transferred onto nitrocellulose membrane (GE Healthcare, Buckinghamshire, UK). The membrane was incubated with 5% dry milk in TBST solution (TBS pH 7.2, 0.1% Tween-20) for 1 h blocking at room temperature, then the primary antibodies (detail and dilution factor were listed below) were diluted with washing solution (2% dry milk in TBST) at 4 °C overnight. On the second day, after 3x of washing with washing solution, the membrane was incubated with secondary horseradish peroxidase-conjugated antibodies (Cell Signaling, Danvers, MA, USA), and signals were detected using a chemiluminescent kit (Santa Cruz Biotechnology, Santa Cruz, CA, USA).

Antibody	Product code	Dilution	Company
aSMA	Ab32575	1:1000	Abcam
a-Tubulin	Sig T5168	1:5000	Sigma
CD31	553370	1:1000	BD Pharmigen
DNMT3a	IMG-268A	1:1000	IMGENEX
Flag	TA50011	1:2500	Origene
HIF1a	MA1-16504	1:1000	Thermal
p-SMAD2	3108s	1:1000	Cell Signaling
p-SMAD3	9520s	1:1000	Cell Signaling
S100A4	HPA007973-100UL	1:1000	Sigma
SMAD2	700048	1:2500	Life Technologies
SMAD3	Ab40854	1:2500	Abcam
SMAD4	Ab40759	1:2500	Abcam

MEDIP-QPCR BASED DETECTION OF METHYLATED RASAL1 PROMOTER

Methylated DNA immunoprecipitation assay was performed as previously described [2,34,35]. Briefly, the total methylated DNA was captured using Methylamp Methylated DNA capture Kit (Epigentek, Farmingdale, NY, USA). A quantity of 1.0 μg of sonicated DNA was used in each reaction and incubated at room temperature for 2 h with gently horizontal shaking. The captured DNA was purified and eluted by 100 μL of nuclease-free water. For each sample, a corresponding input sample was performed using total sonicated DNA served as control. For quantification of methylated RASAL1 promoter, 5 μL of immunoprecipitated DNA with primers (F: GCCCGCCCAGCCTGCTTGTCTGG, R: GGCAGGCAGCGCGCGGCCCTCCACC) and 2x iQ SYBR green Supermix (Bio-Rad, Muenchen, Germany) were used for each PCR reaction in a final volume of 25 μL and ROX was served as passive reference dye (Bio-Rad). The real-time PCR reactions were performed in a 96-well plate format using the Mx3000P qPCR system (Stratagene, Foster City, CA, USA). PCR reaction was manually terminated when the fluorescent signal increased over the threshold. The electrophoresis of PCR products were performed using a Bioanalyzer 2100 (Agilent, Santa Clara, CA, USA) according to the manufacturer's protocol. Electrophoresis results are shown as virtual gel images as described in previous publications [2].

TGFβ2 ELISA ASSAY

Cell medium was collected after hypoxia treatment for 3 days. After centrifugation, the supernatant was transferred transferred into a new tube and used for secretome measurement. The TGFβ2 ELISA assay (Abcam, Cambridge, UK) was performed according to manufacturer's protocol. Briefly, 100 μL of each sample was added into precoated wells and incubated for 3 h at room temperature with gentle shaking. After 4x washing with washing solution, 100 μL of 1x biotinylated TGFβ2 antibody was added into each well and incubated for 1 h at room temperature with gentle shaking. Then each reaction continued with adding 100 μL of 1x HRP-Streptavidin solution for 45 min followed by incubation with 100 μL tetramethylbenzidine substrate reagent for 30 min. A quantity of 50 μL of stop solution was applied to stop the reaction, and then the plate was immediately read by a spectrophotometer (Synergy2; Biotech, Bad Friedrichshall, Germany) at 450 nm wavelength.

STATISTICAL ANALYSIS

Means were calculated and plotted along with standard error bars. All statistical analyses were done using GraphPad PRISM software version 5.0 (GraphPad). All data were first analysed by Student t-test for single comparison and one-way ANOVA for multiple comparisons. Differences between means were considered statistically significant when the P-value ≤ 0.05. Three or more biological replicates were included for all experiments, with the exception of immunofluorescence, which were tested in two independent experiments.

REFERENCES

1. Eisenberg LM and Markwald RR (1995) Molecular regulation of atrioventricular valvuloseptal morphogenesis. Circ Res 77, 1–6.
2 Xu X, Tan X, Tampe B, Nyamsuren G, Liu X, Maier LS, Sossalla S, Kalluri R, Zeisberg M and Hasenfuss G (2015) Epigenetic balance of aberrant rasal1 promoter methylation and hydroxymethylation regulates cardiac fibrosis. Cardiovasc Res 105, 279–291.
3 Maddaluno L, Rudini N, Cuttano R, Bravi L, Giampietro C, Corada M, Ferrarini L, Orsenigo F, Papa E, Boulday G et al. (2013) EndMT contributes to the onset and progression of cerebral cavernous malformations. Nature 498, 492–496.
4 Zeisberg EM, Potenta S, Xie L, Zeisberg M and Kalluri R (2007) Discovery of endothelial to mesenchymal transition as a source for carcinoma-associated fibroblasts. Cancer Res 67, 10123–10128.
5 Zeisberg EM, Potenta SE, Sugimoto H, Zeisberg M and Kalluri R (2008) Fibroblasts in kidney fibrosis emerge via endothelial-to-mesenchymal transition. J Am Soc Nephrol 19, 2282–2287.
6 Zeisberg EM, Tarnavski O, Zeisberg M, Dorfman AL, McMullen JR, Gustafsson E, Chandraker A, Yuan X, Pu WT, Roberts AB et al. (2007) Endothelial-tomesenchymal transition contributes to cardiac fibrosis.Nat Med 13, 952–961.
7 Cuttano R, Rudini N, Bravi L, Corada M, Giampietro C, Papa E, Morini MF, Maddaluno L, Baeyens N, Adams RH et al. (2015) KLF4 is a key determinant in the development and progression of cerebral cavernous malformations. EMBO Mol Med 8, 6–24.
8 Choi SH, Nam JK, Kim BY, Jang J, Jin YB, Lee HJ, Park S, Ji YH, Cho J, Lee YJ et al. (2016) HSPB1 inhibits the endothelial-to-mesenchymal transition to
suppress pulmonary fibrosis and lung tumorigenesis. Cancer Res 21, 3716–3726.
9 Bravi L, Malinverno M, Pisati F, Rudini N, Cuttano R, Pallini R, Martini M, Larocca LM, Locatelli M, Levi V et al. (2016) Endothelial cells lining sporadic cerebral cavernous malformation cavernomas undergo endothelial-to-mesenchymal transition. Stroke 47, 886–890.
10 Peng H, Li Y, Wang C, Zhang J, Chen Y, Chen W, Cao J, Wang Y, Hu Z, Lou T et al. (2016) ROCK1 induces endothelial-to-mesenchymal transition in glomeruli to aggravate albuminuria in diabetic nephropathy. Sci Rep 6, 20304.
11 Mahler GJ, Frendl CM, Cao Q and Butcher JT (2014) Effects of shear stress pattern and magnitude on mesenchymal transformation and invasion of aortic valve endothelial cells. Biotechnol Bioeng 111, 2326–2337.
12 Muylaert DE, de Jong OG, Slaats GG, Nieuweboer FE, Fledderus JO, Goumans MJ, Hierck BP and Verhaar MC (2015) Environmental influences on endothelial to mesenchymal transition in developing implanted cardiovascular tissue-engineered grafts.Tissue Eng Part B Rev 22, 58–67.
13 Rieder F, Kessler SP, West GA, Bhilocha S, de la Motte C, Sadler TM, Gopalan B, Stylianou E and Fiocchi C (2011) Inflammation-induced endothelial-to-mesenchymal transition: a novel mechanism of intestinal fibrosis. Am J Pathol 179, 2660–2673.

14 Tang R, Li Q, Lv L, Dai H, Zheng M, Ma K and Liu B (2010) Angiotensin II mediates the high-glucose-induced endothelial-to-mesenchymal transition in human aortic endothelial cells. Cardiovasc Diabetol 9, 31.

15 Xu X, Tan X, Tampe B, Sanchez E, Zeisberg M and Zeisberg EM (2015) Snail is a direct target of HIF1a in hypoxia-induced endothelial to mesenchymal transition of human coronary endothelial cells. J Biol Chem 290, 16653–16664.

16 Muylaert DE, de Jong OG, Slaats GG, Nieuweboer FE, Fledderus JO, Goumans MJ, Hierck BP and Verhaar MC (2015) Environmental influences on endothelial to mesenchymal transition in developing implanted cardiovascular tissue-engineered grafts. Tissue Eng Part B Rev 22, 58–67.

17 Xu X, Tan X, Tampe B, Sanchez E, Zeisberg M and Zeisberg EM (2015) Snail is a direct target of hypoxia-inducible factor 1alpha (HIF1alpha) in hypoxia-induced endothelial to mesenchymal transition of human coronary endothelial cells. J Biol Chem 290, 16653–16664.

18 Guo X and Wang XF (2009) Signaling cross-talk between TGF-beta/BMP and other pathways. Cell Res 19, 71–88.

19 Krenning G, Barauna VG, Krieger JE, Harmsen MC and Moonen JR (2016) Endothelial plasticity: shifting phenotypes through force feedback. Stem Cells Int 2016, 9762959.

20 Mueller TD and Nickel J (2012) Promiscuity and specificity in BMP receptor activation. FEBS Lett 586, 1846–1859.

21 He WX, Niu ZY, Zhao SL, Jin WL, Gao J and Smith AJ (2004) TGF-beta activated Smad signalling leads to a Smad3-mediated down-regulation of DSPP in an odontoblast cell line. Arch Oral Biol 49, 911–918.

22 Zeisberg M, Hanai J, Sugimoto H, Mammoto T, Charytan D, Strutz F and Kalluri R (2003) BMP-7 counteracts TGF-beta1-induced epithelial-to-mesenchymal transition and reverses chronic renal injury. Nat Med 9, 964–968.

23 Choi SH, Hong ZY, Nam JK, Lee HJ, Jang J, Yoo RJ, Lee YJ, Lee CY, Kim KH, Park S et al. (2015) A hypoxia-induced vascular endothelial-to-mesenchymal transition in development of radiation-induced pulmonary fibrosis. Clin Cancer Res 21, 3716–3726.

24 Curci C, Castellano G, Stasi A, Divella C, Loverre A, Gigante M, Simone S, Cariello M, Montinaro V, Lucarelli G et al. (2014) Endothelial-to-mesenchymal transition and renal fibrosis in ischaemia/reperfusion injury are mediated by complement anaphylatoxins and Akt pathway. Nephrol Dial Transplant 29, 799–808.

25 Higgins DF, Kimura K, Iwano M and Haase VH (2008) Hypoxia-inducible factor signaling in the development of tissue fibrosis. Cell Cycle 7, 1128–1132.

26 Greer SN, Metcalf JL, Wang Y and Ohh M (2012) The updated biology of hypoxia-inducible factor. EMBO J 31, 2448–2460.

27 Weidemann A and Johnson RS (2008) Biology of HIF-1alpha. Cell Death Differ 15, 621–627.

28 Miyazaki K, Kawamoto T, Tanimoto K, Nishiyama M, Honda H and Kato Y (2002) Identification of functional hypoxia response elements in the promoter region of the DEC1 and DEC2 genes. J Biol Chem 277, 47014–47021.

29 Shu Y, Liu Y, Li X, Cao L, Yuan X, Li W and Cao Q (2016) Aspirin-triggered resolvin D1 inhibits TGFbeta1-induced EndMT through increasing the expression of Smad7 and is closely related to oxidative stress. Biomol Ther (Seoul) 24, 132–139.

30 Akman HO, Zhang H, Siddiqui MA, Solomon W, Smith EL and Batuman OA (2001) Response to hypoxia involves transforming growth factor-beta2 and Smad proteins in human endothelial cells. Blood 98, 3324–3331.

31 Zhang H, Akman HO, Smith EL, Zhao J, Murphy-Ullrich JE and Batuman OA (2003) Cellular response to hypoxia involves signaling via Smad proteins. Blood 101, 2253–2260.

32 Katsura A, Suzuki HI, Ueno T, Mihira H, Yamazaki T, Yasuda T, Watabe T, Mano H, Yamada Y and Miyazono K (2016) MicroRNA-31 is a positive modulator of endothelial-mesenchymal transition and associated secretory phenotype induced by TGF-beta. Genes Cells 21, 99–116.

33 Bechtel W, McGoohan S, Zeisberg EM, Muller GA, Kalbacher H, Salant DJ, Muller CA, Kalluri R and Zeisberg M (2010) Methylation determines fibroblast activation and fibrogenesis in the kidney. Nat Med 16, 544–550.

34 Tampe B, Tampe D, Muller CA, Sugimoto H, LeBleu V, Xu X, Muller GA, Zeisberg EM, Kalluri R and Zeisberg M (2014) Tet3-mediated hydroxymethylation of epigenetically silenced genes contributes to bone morphogenic protein 7-induced reversal of kidney fibrosis. J Am Soc Nephrol 25, 905–912.

35 Xu X, Friehs I, Zhong Hu T, Melnychenko I, Tampe B, Alnour F, Iascone M, Kalluri R, Zeisberg M, Del Nido PJ et al. (2015) Endocardial fibroelastosis is caused by aberrant endothelial to mesenchymal transition. Circ Res 116, 857–866.

36 Tampe B, Tampe D, Zeisberg EM, Muller GA, Bechtel-Walz W, Koziolek M, Kalluri R and Zeisberg M (2015) Induction of Tet3-dependent epigenetic remodeling by low-dose hydralazine attenuates progression of chronic kidney disease. EBioMedicine 2, 19–36.

37 Moore-Morris T, Guimaraes-Camboa N, Banerjee I, Zambon AC, Kisseleva T, Velayoudon A, Stallcup WB, Gu Y, Dalton ND, Cedenilla M et al. (2014) Resident fibroblast lineages mediate pressure overload-induced cardiac fibrosis. J Clin Invest 124, 2921–2934.

38 Kawabata M, Inoue H, Hanyu A, Imamura T and Miyazono K (1998) Smad proteins exist as monomers in vivo and undergo homo- and hetero-oligomerization upon activation by serine/threonine kinase receptors. EMBO J 17, 4056–4065.

39 Saha A, Jha HC, Upadhyay SK and Robertson ES (2015) Epigenetic silencing of tumor suppressor genes during in vitro Epstein-Barr virus infection. Proc Natl Acad Sci USA 112, E5199–E5207.

40 Minami K, Chano T, Kawakami T, Ushida H, Kushima R, Okabe H, Okada Y and Okamoto K (2010) DNMT3L is a novel marker and is essential for the growth of human embryonal carcinoma. Clin Cancer Res 16, 2751–2759.

41 Hao S, He W, Li Y, Ding H, Hou Y, Nie J, Hou FF, Kahn M, Liu Y (2011) Targeted inhibition of betacatenin/CBP signaling ameliorates renal interstitial fibrosis. J Am Soc Nephrol 22, 1642–1653.

42 Yu H, Mrowietz U and Seifert O (2009) Downregulation of SMAD2, 4 and 6 mRNA and TGFbeta receptor I mRNA in lesional and non-lesional psoriatic skin. Acta Derm Venereol 89, 351–356.

43 Wang LH, Kim SH, Lee JH, Choi YL, Kim YC, Park TS, Hong YC, Wu CF and Shin YK (2007) Inactivation of SMAD4 tumor suppressor gene during gastric carcinoma progression. Clin Cancer Res 13, 102–110.

44 Xu X, Pantakani DK, Lührig S, Tan X, Khromov T, Nolte J, Dressel R, Zechner U and Engel W (2011) Stagespecific germ-cell marker genes are expressed in all mouse pluripotent cell types and emerge early during induced pluripotency. PLoS One 6, e22413.